Vocal fold dynamics in a synthetic self-oscillating model: Contact pressure and dissipated-energy dose

Mohsen Motie-Shirazi, Matías Zañartu, Sean D. Peterson, and Byron D. Erath

Citation: The Journal of the Acoustical Society of America **150**, 478 (2021); doi: 10.1121/10.0005596
View online: https://doi.org/10.1121/10.0005596
View Table of Contents: https://asa.scitation.org/toc/jas/150/1
Published by the Acoustical Society of America

JASA ARTICLE

Vocal fold dynamics in a synthetic self-oscillating model: Contact pressure and dissipated-energy dose

Mohsen Motie-Shirazi,[1,a)] Matías Zañartu,[2,b)] Sean D. Peterson,[3,c)] and Byron D. Erath[1,d)]
[1]Department of Mechanical and Aeronautical Engineering, Clarkson University, Potsdam, New York 13699, USA
[2]Department of Electronic Engineering, Universidad Técnica Federico Santa María, Valparaíso, Chile
[3]Department of Mechanical and Mechatronics Engineering, University of Waterloo, Waterloo, Ontario, Canada

ABSTRACT:
The energy dissipated during vocal fold (VF) contact is a predictor of phonotrauma. Difficulty measuring contact pressure has forced prior energy dissipation estimates to rely upon generalized approximations of the contact dynamics. To address this shortcoming, contact pressure was measured in a self-oscillating synthetic VF model with high spatiotemporal resolution using a hemilaryngeal configuration. The approach yields a temporal resolution of less than 0.26 ms and a spatial resolution of 0.254 mm in the inferior-superior direction. The average contact pressure was found to be 32% of the peak contact pressure, 60% higher than the ratio estimated in prior studies. It was found that 52% of the total power was dissipated due to collision. The power dissipated during contact was an order of magnitude higher than the power dissipated due to internal friction during the non-contact phase of oscillation. Both the contact pressure magnitude and dissipated power were found to be maximums at the mid anterior-posterior position, supporting the idea that collision is responsible for the formation of benign lesions, which normally appear at the middle third of the VF. © *2021 Acoustical Society of America*. https://doi.org/10.1121/10.0005596

(Received 2 December 2020; revised 18 June 2021; accepted 21 June 2021; published online 21 July 2021)
[Editor: Zhaoyan Zhang] Pages: 478–489

I. INTRODUCTION

Repeated vocal fold (VF) collision during phonation produces a surface contact pressure that imparts stresses acting perpendicularly to the tissue load-bearing fibers.[1] Therefore, abnormally high contact pressure is believed to play a primary role in VF damage by harming the basement membrane,[2] which may lead to development of some structural VF pathologies, such as polyps and nodules.[3] Consequently, the peak contact pressure, which usually occurs at the middle of the contact zone,[4] is considered an important metric for identifying the formation of benign lesions.

Vocal dose denotes the accumulated exposure of the VF tissue to vibration[5,6] and aims to quantify long timescale VF damage. The collision dissipated-energy dose is defined as the total energy dissipated due to collision of the VFs.[7] As such, it has been proposed as a measure for assessing the risk of phonotraumatic VF damage due to VF fatigue and injury.[7] To calculate the collision dissipated-energy dose, the measured contact pressure signal must be acquired at a spatiotemporal resolution that is significantly finer than the VF contact length scale [$\mathcal{O}(1\,\text{mm})$], and the contact duration [$\mathcal{O}(1\text{ ms})$]. Due to the difficulty of acquiring these measures,[2,8,9] prior efforts have been forced to rely upon gross estimates of the contact dynamics. This poses additional challenges as the predicted damage can be highly sensitive to these estimates.[7] Although a significant body of work has focused on quantifying VF contact mechanics,[4,10,11] comprehensive measurements that are capable of accurately predicting vocal dose remain elusive.

A variety of modalities have been explored to resolve contact pressure. *In vivo* peak contact pressure has been directly investigated in a large number of studies,[12–15] although measurement accuracy has proven problematic, as it requires repeatable, periodic VF oscillations. Fabrication of a sufficiently small sensor with an appropriate frequency response to provide the desired spatial and temporal resolution within the small VF contact zone is a significant challenge.[16] Peak contact pressure measurements have been acquired in excised larynges *via* direct measurement with physical sensors,[4,17] as well as indirect estimation based on digital image correlation (DIC).[18] Most notable is the seminal work of Jiang and Titze,[4] where the temporally-varying dynamics of contact were elucidated, identifying an impulse-like pressure peak with a magnitude that is generally higher than the subglottal pressure. Unfortunately, the relatively large sensor size diminished the spatial resolution of the contact pressure measurements. Self-oscillating silicone VF models have also been employed to determine contact dynamics, using both direct[11,19] and indirect measures via DIC,[20] although the high experimental uncertainties associated with the measurement techniques employed in these studies have led to questions regarding their validity.[16] Computational models, which are not constrained by experimental limitations, have found broader use in contact

a)ORCID: 0000-0002-0168-0330.
b)ORCID: 0000-0001-5581-4392.
c)ORCID: 0000-0001-8746-2491.
d)Electronic mail: berath@clarkson.edu, ORCID: 0000-0003-0057-6731.

https://doi.org/10.1121/10.0005596

pressure investigations.[21–25] However, the universal shortcoming is that a collision model must be prescribed, and the experimental contact measures against which these approaches can be validated are limited.

Recently, a new approach for measuring intraglottal aerodynamic and contact pressures with synthetic, self-oscillating VF models in a hemilaryngeal configuration was developed and validated.[16] The self-oscillating VF model captures both three-dimensional and unsteady flow effects, and the measurement technique provides high spatial and temporal resolution of the intraglottal pressure field.

The aim of this work is to directly compute the VF contact pressure and resultant vocal dose using the experimental framework of Motie-Shirazi *et al.*[16] In addition, the ratio of average to peak contact pressure and the dissipated fraction of the VF energy during the contact phase are investigated to enable estimation of vocal dose based on VF kinematics. Section II is devoted to the introduction and analysis of dissipated-power dose; the flow facility and methods are introduced in Sec. III; the results are presented in Sec. IV and discussed in Sec. V, while Sec. VI is left for the conclusions.

II. ANALYSIS OF POWER TRANSFER DURING COLLISION

A. Dissipated power

Dissipated-energy dose, which can be used as a measure of VF damage,[5] can be divided into two parts: the energy dissipated by friction in the VF tissue due to viscosity, and the energy dissipated during collision.[7] The ratio of dissipated energy during collision to the total VF energy can then be expressed as a dissipation coefficient. The coefficient can also be expressed in terms of power by dividing the energies by the period of oscillation, such that

$$C = \frac{\dot{W}_{\mathrm{d}}}{\dot{W}_{\mathrm{T}}}, \tag{1}$$

where $\dot{W}_{\mathrm{d}}$ is the dissipated power per unit volume, and $\dot{W}_{\mathrm{T}}$ is the total VF power per unit volume immediately preceding contact. Because all parameters discussed herein are computed over a per unit period of oscillation, subsequent analysis will be performed based on power. Furthermore, although all subsequent discussions are on a per unit volume basis, the text will only refer to the fundamental variable for brevity.

In their initial formulation for the dissipation coefficient, C, Titze and Hunter[7] assumed that the dissipated power was equal to the power transferred to the VFs during contact, $\dot{W}_{\mathrm{cont}}$, and the total power immediately preceding contact was approximated by the kinetic power of the oscillating VFs, $\dot{W}_{\mathrm{k}}$. They then estimated the kinetic power of the VF as $\dot{W}_k = (1/2)Q_{\mathrm{c}}\rho\omega^2 l_{\mathrm{g,w}}^2 f_o$, where Q_{c} is the closed quotient, ρ is the density of the VF tissue, ω is the angular velocity, $l_{\mathrm{g,w}}$ is the amplitude of oscillation, and f_o is the oscillation frequency. The dissipation coefficient was then approximated as

$$C = \frac{\dot{W}_{\mathrm{cont}}}{\dot{W}_{\mathrm{k}}} = \frac{p_{\mathrm{cont,avg}}/T}{\frac{1}{2}Q_{\mathrm{c}}\rho\omega^2 l_{\mathrm{g,w}}^2 f_o}. \tag{2}$$

The units of dissipated power, which arises due to contact, can be expressed as Pa/s and it was therefore argued that this could be expressed as the mean contact pressure, $p_{\mathrm{cont,avg}}$, divided by the period of oscillation, T. The advantage of this formulation is that if the dissipation coefficient, C, is known, the dissipated collision power (i.e., the collision dose) can be computed solely from kinematic parameters of the VF oscillation. This coefficient was then computed based on estimates of VF contact pressure and kinematic parameters reported in prior excised VF studies, namely, $p_{\mathrm{cont,avg}} = 1.0$ kPa, $Q_{\mathrm{c}} = 0.5$, $\rho = 1020\ \mathrm{kg/m^3}$, $l_{\mathrm{g,w}} = 1.0$ mm, and $f_o = 160$ Hz. Plugging these values into Eq. (2) gives $C = 3.88$. However, they erroneously reported this coefficient to be $C = 0.02$. It appears an error was made as this value is only arrived at if $p_{\mathrm{cont,avg}}$ is not divided by T in the numerator of Eq. (2), which produces a dimensionally inconsistent result if used this way. The value of $C = 3.88$ is, however, nonphysical, since by definition $0 \le C \le 1$, suggesting that there is a flaw in the analysis.

To uncover the flaw, an energy budget analysis during contact is performed, noting that the total energy prior to contact, which is assumed to be fully-captured by the VF kinetic energy, must equal the total energy of the VF at the point that it stops moving. The energy transferred to the VF during contact can be expressed in terms of an elastic component, which restores energy to the VFs during collision, and a viscous dissipation component, capturing energy lost during the event. Dividing the energy by the period of oscillation to obtain the corresponding power, this can be expressed as

$$\dot{W}_{\mathrm{d}} = \dot{W}_{\mathrm{T}} - \dot{W}_{\mathrm{cont}}, \tag{3}$$

where $\dot{W}_{\mathrm{cont}}$ is the purely potential elastic component of the contact, which can be computed as the product of the average contact force, $F_{\mathrm{cont,avg}}$ and a fictitious medial-lateral penetration depth of the VF due to contact, δ_{cont}, divided by the VF volume and the oscillation period, such that

$$\dot{W}_{\mathrm{cont}} = \frac{F_{\mathrm{cont,avg}}\delta_{\mathrm{cont}}}{A_{\mathrm{cont}} l_{\mathrm{VF,w}} T} = \frac{p_{\mathrm{cont,avg}}}{T}\frac{\delta_{\mathrm{cont}}}{l_{\mathrm{VF,w}}}. \tag{4}$$

Similar to the previous work,[5] the volume of the VF can be approximated by a parallelepiped having a constant cross-sectional area, A_{cont}, equal to the area of contact, and a medial-lateral width of $l_{\mathrm{VF,w}}$.

This formulation identifies an additional nuance. Comparing Eq. (4) with the numerator of Eq. (2), as formulated in Titze and Hunter,[7] reveals that although both equations are dimensionally consistent, Eq. (4) correctly includes a nondimensionalized distance over which the force acts, $\delta_{\mathrm{cont}}/l_{\mathrm{VF,w}}$. By excluding this term in the prior theory, it is inherently implied that its value is 1, which is representative of the contact force displacing the VF a distance equal to the medial-lateral width. In reality, the nondimensionalized deformation distance should be much less, but the precise value remains to be determined.

Returning to the updated formulation for computing the dissipated power, Eq. (3), the total power can further be expressed as the VF kinetic power, $\dot{W}_{\mathrm{k}}$, immediately preceding contact. The potential elastic power preceding contact, which is stored due to the VF adduction, is not included in the total power because this form of energy is only a function of the medial compression of the VF, which remains unchanged during VF collision. Substituting the kinetic power into Eq. (3), combining it with Eq. (4), and then substituting into Eq. (1) yields

$$C = \frac{\dot{W}_{\mathrm{k}} - \dot{W}_{\mathrm{cont}}}{\dot{W}_{\mathrm{k}}} = 1 - \frac{\dfrac{p_{\mathrm{cont,avg}}}{T}\dfrac{\delta_{\mathrm{cont}}}{l_{\mathrm{VF,w}}}}{\dot{W}_{\mathrm{k}}}. \tag{5}$$

Note, the kinetic power can still be expressed in terms of the VF kinematics (see Sec. II B), but additional information is needed to solve for the dissipated power coefficient, C. Namely, the average contact pressure, $p_{\mathrm{cont,avg}}$, and the VF medial-lateral deformation distance during contact, δ_{cont}, which must be estimated.

The method of calculating the values for each of the terms in Eq. (5) is introduced in the following sections, leading to an updated prescription of the dissipated power coefficient, C.

B. VF kinetic power

The total VF kinetic power, $\dot{W}_{\mathrm{k}}$, is estimated based on the medial VF surface velocity immediately preceding contact, V_{cont}. Prior studies showed that for a VF with a stiff body and a soft cover layer, the oscillation amplitude is much greater within the cover layer and decays in the body layer.[26] However, the internal displacement and velocity profile of the VF have not been well quantified in the literature. To estimate the kinetic power of the VF, it is assumed that the tissue velocity within the VF decreases quadratically as a function of distance from the VF medial surface and reaches a value of zero at the lateral face of the VF, defined in Sec. III B as the lateral surface of the adipose tissue layer. In addition, the inferior-superior thickness of the VF, $l_{\mathrm{VF,t}}$, varies as a function of the distance from the lateral face of the VF model, z. This gives

$$\dot{W}_{\mathrm{k}} = \frac{1}{A\, l_{\mathrm{VF,l}}\, T}\int_0^{l_{\mathrm{VF,w}}} \frac{1}{2}\rho\left(V_{\mathrm{cont}}\left(\frac{z}{l_{\mathrm{VF,w}}}\right)^2\right)^2 l_{\mathrm{VF,l}}\, l_{\mathrm{VF,t}}(z)\,\mathrm{d}z, \tag{6}$$

where A is the coronal cross-sectional area of the VF model, $l_{\mathrm{VF,l}}$ is the anterior-posterior length of the VF, T is the oscillation period, $l_{\mathrm{VF,w}}$ is the medial-lateral width of the VF, ρ is the average density of the VF, and V_{cont} is the average VF surface velocity immediately preceding contact, which is estimated based on kymogram plots of the VF, as will be discussed in Sec. IV C 1.

C. Contact power

The contact power, $\dot{W}_{\mathrm{cont}}$, was previously defined as the elastic component of energy during VF collision, per period of oscillation [see Sec. II A and Eq. (3)]. It can be calculated based on the work done on the VF by the average contact pressure, divided by the total volume of the VF, $\rlap{-}V$, and the oscillation period. Therefore, it is found according to

$$\dot{W}_{\mathrm{cont}} = \frac{F_{\mathrm{cont,avg}}\,\delta_{\mathrm{cont}}}{\rlap{-}V T} = \frac{p_{\mathrm{cont,avg}} A_{\mathrm{cont,avg}}\,\delta_{\mathrm{cont}}}{A\, l_{\mathrm{VF,l}}\, T}, \tag{7}$$

where $F_{\mathrm{cont,avg}}$, $p_{\mathrm{cont,avg}}$, and $A_{\mathrm{cont,avg}}$ are the average contact force, pressure, and area during the contact phase, respectively, and δ_{cont} is the fictitious penetration depth of the VF during contact that yields the resultant contact pressure. This will be found assuming a Hertzian model of contact. Crucially, calculating the values of $p_{\mathrm{cont,avg}}$, $A_{\mathrm{cont,avg}}$, and δ_{cont} requires measurements of the contact pressure with sufficiently high spatial and temporal resolution. Consequently, an experimental campaign is undertaken to obtain these values and to simultaneously explore the spatiotemporal mechanics of VF contact.

III. METHODS

A. Flow facility

Contact pressure measurements were acquired using a synthetic, self-oscillating VF model in a hemilarynegal flow facility, which was similar to that employed in prior work.[16] A schematic of the experimental facility is shown in Fig. 1(a). The details of the facility have been previously reported,[16,27] and are only discussed briefly herein. Pressurized air was regulated to 17 kPa by a Siemens 40-2 pressure regulator (Siemens, Munich, Germany) prior to entering a Dwyer RMC 103-SSV flow meter (Dwyer, Michigan City, IN) that adjusted the upstream air pressure and measured the time-averaged flow rate. The airflow then entered a 0.03 m^3 plenum chamber with a cross-sectional area of 0.06 m^2 that was acoustically insulated by securing 2 cm thick foam to the inner walls. The flow exited the plenum chamber into a rectangular channel with a length of 150.0 mm and a cross-sectional area of 213.0 mm^2, representing the trachea. A Kulite ET-3DC pressure transducer (Kulite, Leonia, NJ) measured the unsteady subglottal pressure at a distance of 30.0 mm from the channel exit.

At the end of the tracheal channel, a bracket with a rectangular cut-out that holds the VF model was bolted to the channel exit. The VF model oscillated against a movable flat contact plate that formed the medial surface of the tracheal wall, thereby creating a hemilaryngeal configuration. The anterior-posterior length was 17.0 mm. A Millar-Mikro-Cath pressure sensor (Millar, Houston, TX) was embedded in a groove under the surface of the hemilarynegal plate such that the sensing element was positioned beneath a 1.3 mm by 1.5 mm window that was open to the

https://doi.org/10.1121/10.0005596

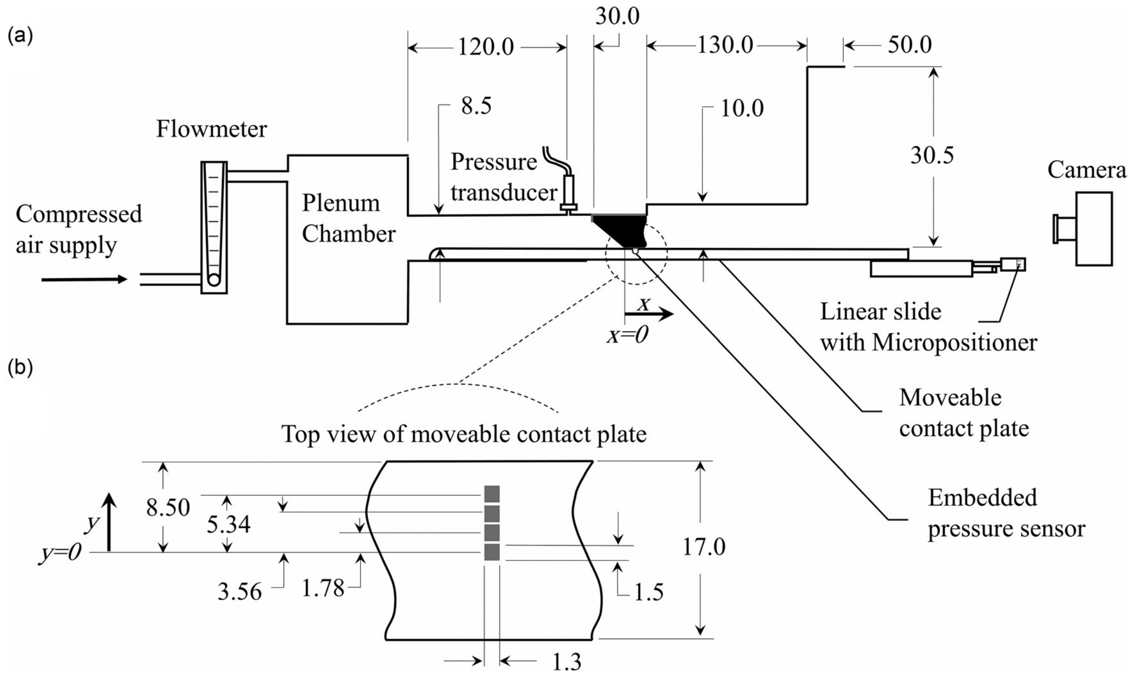

FIG. 1. (a) Schematic of the experimental flow facility. (b) A close-up top view of the contact plate and the relative position of the pressure sensors. All dimensions are in mm.

surface of the plate. The groove was filled with Smooth-On Dragon Skin 10 silicone (Smooth-On Inc., Macungie, PA) to create a flat contact surface, with the silicone transmitting the pressure to the sensor. This method for measuring the intraglottal pressure was validated in Ref. 16. The frequency response of the Millar pressure transducer in this configuration was found to be greater than 3.8 kHz,[16] yielding a temporal resolution of better than 0.26 ms for contact pressure measurements. The superior end of the hemilaryngeal plate was connected to a Thorlabs PT1 linear slide (Thorlabs, Newton, NJ) that enabled movement of the plate in the inferior-superior direction and, thereby, adjustment of the embedded sensor position with an accuracy of 0.0254 mm, although the measurements were performed with an increment of 0.254 mm. The x coordinate corresponds to the inferior-superior distance from the inferior edge of the glottis when the VF was at rest. Four separate contact plates were fabricated with a separate pressure sensor embedded at a different anterior-posterior location in each plate, as measured from the midline, and indicated by the y coordinate. In this manner, interchanging contact plates in the facility enabled measurement of the contact pressure at locations of $y = 0$, 1.78, 3.56, and 5.34 mm, as shown in Fig. 1(b).

A simplified vocal tract was attached to the superior exit of the VF with an idealized cross-sectional area similar to a human vocal tract producing the vowel /o/.[28] The vocal tract had a total height of 180.0 mm in the inferior-superior direction and a length of 26.2 mm in the anterior-posterior direction. It consisted of two connected channels with different medial-lateral widths, similar to the vocal tract used in prior investigations.[29] The inferior portion of the tract had a constant rectangular cross-sectional area of 262.0 mm^2 over a height of 130.0 mm, representing the epilaryngeal tube. It was connected superiorly to another section with a constant rectangular cross-sectional area of 799.1 mm^2 over a height of 50.0 mm, representing the oral cavity. Unfortunately, the similarity between the acoustic behavior of this simplified vocal tract geometry and the human vocal tract was not investigated in this study. This remains the subject of future work.

A Photron AX200 high-speed camera (Photron, Tokyo, Japan) with an Elicar V-HQ Macro 90 mm f 2.5 lens (Jaca Corporation, Tokyo, Japan) was positioned 300.0 mm superior to the VF exit and recorded high-speed video (HSV) of the VF oscillations. The video was recorded at 20 000 frames-per-second and with a spatial resolution of 0.075 mm/pixel. The subglottal and contact pressures were acquired simultaneously with a National Instruments PCIe-6321 data acquisition card and a custom LabVIEW program (National Instruments Corporation, Austin, TX) at a sampling rate of 80 kHz over a total acquisition time of 0.75 s. A custom LabVIEW program was used to synchronize the pressure measurements and HSV recordings.

B. VF model

A four-layer synthetic VF model was fabricated from silicone rubber with the same geometry, material, and mixture ratios as previously reported.[16] A schematic of the coronal cross section of the model layers is shown in Fig. 2, with a more detailed description provided in Ref. 16, including the mixture ratios for each layer. The model had a uniform profile in the anterior-posterior direction with a length of 17.0 mm.

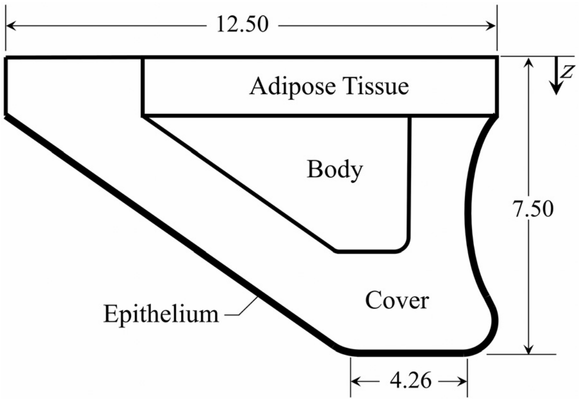

FIG. 2. Geometry and key dimensions of the synthetic VF model. All dimensions are in mm.

Note that all of the lengths in the text are presented by the symbol "l" with two subscripts. The first subscript denotes the glottal dimensions, g, or the VF dimensions, VF. The second subscript of l, w, or t indicates the anatomical directions along the anterior-posterior, medial-lateral, and inferior-superior axes, respectively. For instance, the VF model had an anterior-posterior length of $l_{\mathrm{VF,l}} = 17.0$ mm, a medial-lateral width of $l_{\mathrm{VF,w}} = 7.50$ mm, and an inferior-superior thickness of $l_{\mathrm{VF,t}}$, which varied from 12.50 mm at the lateral surface to 4.26 mm at the medial surface. The glottal length was equal to the VF length, $l_{\mathrm{g,l}} = l_{\mathrm{VF,l}}$, and the glottal thickness was equal to the VF thickness at the medial surface, $l_{\mathrm{g,t}} = 4.26$ mm.

Elastic and viscous shear moduli of each layer of the VF model were measured with a TA Instruments AR 2000 Rheometer (TA Instruments, New Castle, DE) at 1% strain for 20 frequencies between 1 and 100 Hz. The magnitude of the complex modulus of elasticity of each layer was calculated at a frequency of 100 Hz and is presented with the reported range of physiological values in Table I. The measured moduli of the silicone layers were all within the physiological range.

To ensure robust collision during VF oscillation, a medial prephonatory compression of 0.75 mm was applied to the VF model, which resulted in a medial prephonatory pressure of 1.25 kPa. The medial prephonatory compression is the amount the VF is compressed in the medial-lateral direction against the contact plate when the VF is at rest, and the medial prephonatory pressure is the resulting surface pressure.[16]

TABLE I. Moduli of elasticity of physiological and silicone vocal fold models for each layer.

Layer	Physiological range (kPa)	Silicone VF Model (kPa)
Adipose tissue	1–10 (Ref. 30)	4.04
Body	1.5–50 (Refs. 31–33)	7.13
Cover	1–8 (Refs. 32,34–38)	1.10
Epithelium	Not measured	81.10

C. Contact pressure measurement

Each of the four hemilaryngeal plates were initially placed with the sensor located at $x = 21.62$ mm, superior to the VF contact region. The sensor was then moved inferiorly in increments of 0.254 mm until reaching the inferior position of $x = -4.78$ mm, yielding a total of 104 pressure measurements in the inferior-superior direction at each anterior-posterior position. The pressure magnitude at each position was measured as a function of time for 0.75 s. The measured pressure waveforms in the inferior-superior direction were synchronized and phase-averaged by identifying the start of each individual oscillation cycle, referenced by the unchanging subglottal pressure waveform.

IV. RESULTS

A. Oscillation dynamics

The VF had an onset pressure of 1.70 kPa. The contact measurements were performed for a mean subglottal pressure of $p_{\mathrm{sub}} = 2.20$ kPa, which produced a mean flow rate of 338 mL/s. The fundamental frequency was 160 Hz, which resulted in a period of $T = 6.25$ ms, producing approximately 120 oscillation cycles over the 0.75 s acquisition time.

A kymogram at the VF midline was extracted from the HSV (not shown for brevity), from which the open and speed quotients were computed to be 0.78 and 2.09, respectively. Both of these values are within the range of physiological values.[39,40] The maximum medial-lateral glottal width and glottal area were calculated to be 0.67 mm and 8.45 mm^2, respectively, which are also physiologically relevant.[41,42] The onset pressure was higher than the physiological value of approximately 0.5 kPa,[43] which also led to a higher than normal flow rate. This is likely because of two reasons. First, it has been shown that employing VFs in a hemilaryngeal flow facility results in an increase in the onset pressure.[4,10,17,44] Second, because synthetic VF models do not normally exhibit complete closure,[11,44] a medial prephonatory compression was applied to the VFs to achieve robust collision, which also increased the onset pressure. Nevertheless, the kinematic features of the VF oscillations were representative of physiological behavior.

B. Contact pressure

The spatial variation of the normalized pressure drop relative to the mean subglottal pressure, $(p - p_{\mathrm{sub}})/p_{\mathrm{sub}}$, is plotted in Figs. 3(a)–3(d) at the four anterior-posterior locations of interest, and at four different instances in time as VF closure progresses. The inferior-superior distance, x, is normalized by the inferior-superior glottal thickness of the VF at rest and before applying the medial compression, defined as $l_{\mathrm{g,t}} = 4.26$ mm (see Fig. 2). The anterior-posterior distance, y, is normalized by the glottal half length in the anterior-posterior direction, $l_{\mathrm{g,l}}/2 = 0.85$ mm, and the time, t, is normalized by the period of an oscillation cycle, T. The time is adjusted such that at $t/T = 0.0$, the VF is at

https://doi.org/10.1121/10.0005596

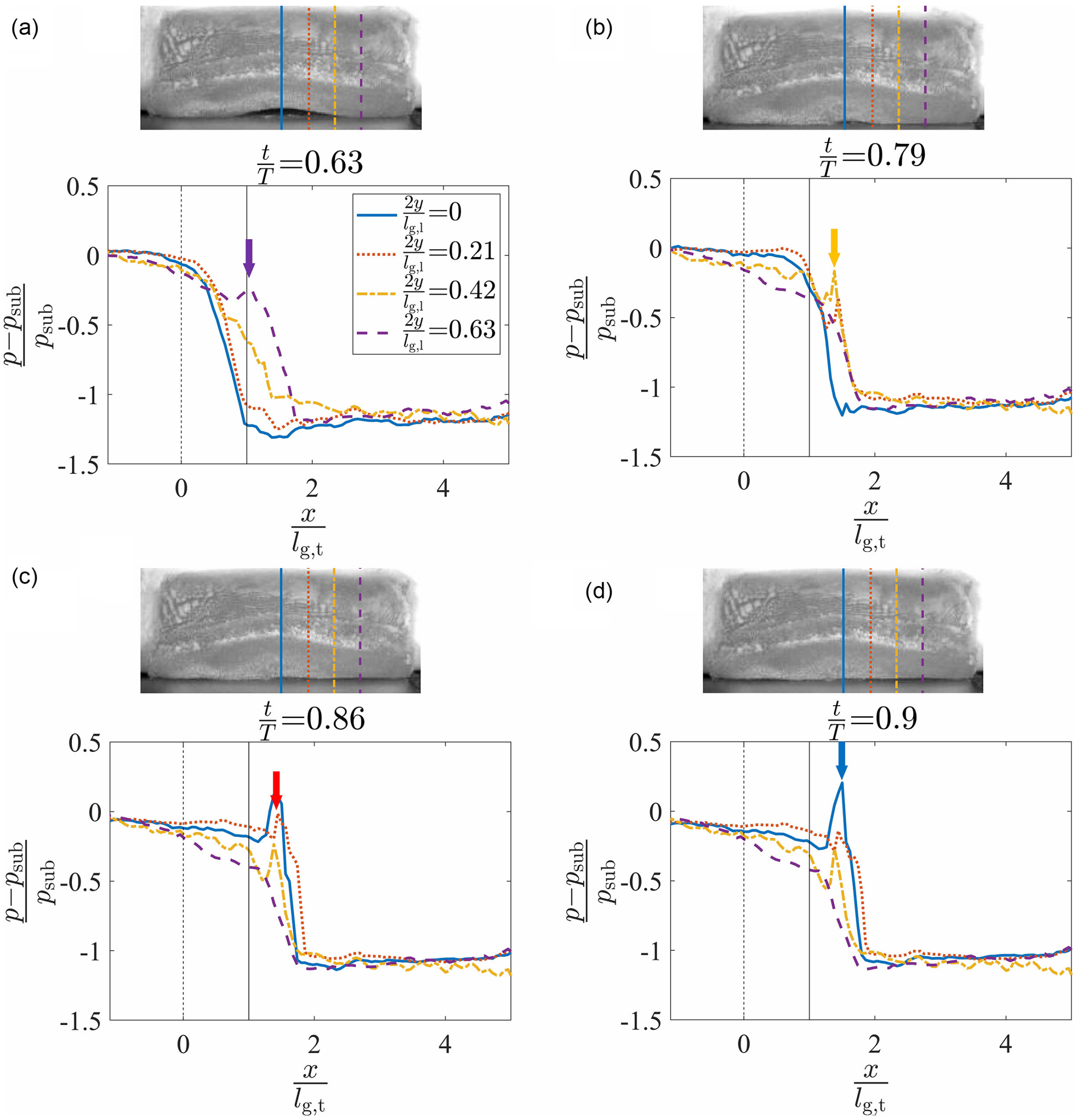

FIG. 3. (Color online) The normalized pressure drop versus the normalized inferior-superior distance, plotted at four positions in the anterior-posterior direction, and at the normalized times of (a) $t/T = 0.63$, (b) $t/T = 0.79$, (c) $t/T = 0.86$, and (d) $t/T = 0.90$. The times coincide with the maximum contact pressure of the VF at the anterior measurement locations, indicated by an arrow, at (a) $2y/l_{g,l} = 0.63$, (b) $2y/l_{g,l} = 0.42$, (c) $2y/l_{g,l} = 0.21$, and (d) $2y/l_{g,l} = 0.0$. Each inset presents a superior view of the VF orientation at that specific instance in time. Dashed and solid vertical lines at $x/l_{g,t} = 0$ and $x/l_{g,t} = 1$, respectively, identify the glottal entrance and exit when the VF is in its rest configuration.

the beginning of the opening phase. Also included are superior view images of the VF at the corresponding time with overlaid lines indicating the anterior position of the spatial pressure measurement locations.

In Fig. 3(a), the VF is open at the midline but closure has occurred at the most anterior position of $2y/l_{g,l} = 0.63$. This can be observed in the plot by noting that at the inferior position along the VF surface ($x/l_{g,t} = -1$), the pressure is approximately equal to the subglottal pressure. Moving superiorly, the pressure at $2y/l_{g,l} = 0.63$ slowly decreases, followed by a sudden rise to a local maxima, as indicated by an arrow. This peak indicates VF contact, which occurs due to a sudden change in the VF momentum.[4,16] The point of local minimum of the pressure distribution preceding the peak identifies the inferior edge of the contact area, while the superior edge is demarcated by the location at which the intraglottal pressure reaches the constant supraglottal pressure ($x/l_{g,t} \approx 2$). The progression of contact can be tracked in time by following the variation in the contact pressure peak, as clearly identified in the supplementary video,[45] which presents the time-varying intraglottal pressure distribution during contact with a temporal resolution of $t/T = 0.01$.

Subsequent time points in Fig. 3 track the spatiotemporal progression of contact as it moves towards the midline, evidenced by peaks in the contact pressure at successive anterior locations of $2y/l_{g,l} = 0.63$, 0.42, 0.21, and 0.0. The maximum contact pressure, $p_{cont,max}$, occurring at each of the anterior locations, is denoted by an arrow. Comparing the inferior-superior position of the contact peak across anterior-posterior positions highlights the three-dimensional nature of the contact evolution, wherein contact near the midline occurs at a more superior location as the VF bulges in that direction. Specifically, the maximum contact pressure, $p_{\mathrm{cont,max}}$, occurred at inferior-superior locations of $x/l_{\mathrm{g,t}} = 1.02$, 1.38, 1.44, and 1.50 for the anterior-posterior positions of $2y/l_{\mathrm{g,l}} = 0.0, 0.21, 0.42$, and 0.63, respectively. The progression of the pressure distribution also shows that the VF contact peak vanished sooner at the more anterior locations. This can be observed in Fig. 3(d), in which the peak in the pressure distribution is visible at all of the anterior locations, except at $2y/l_{\mathrm{g,l}} = 0.63$. This denotes that the VF opening, and consequently the contact, started from the more anterior positions and moved toward the midline, which is also obvious in the supplementary video.

The maximum contact pressure, $p_{\mathrm{cont,max}}$, also varied in the anterior-posterior position. Figure 4 indicates the normalized value of $p_{\mathrm{cont,max}}/p_{\mathrm{sub}}$. The highest value of contact pressure occurred at the midline with $p_{\mathrm{cont,max}} = 2.72$ kPa and a standard deviation of 0.06 kPa, and decreased in the anterior direction, with the value at $2y/l_{\mathrm{g,l}} = 0.63$ being approximately 40% of that at the midline. The ratio of peak contact pressure to subglottal pressure of $p_{\mathrm{cont,max}}/p_{\mathrm{sub}} = 1.24$ was within the span of previously reported values that ranged from approximately 1.0 to 2.0.[4,17]

1. Average contact pressure

Calculating the contact power, $\dot{W}_{\mathrm{cont}}$, from Eq. (7) requires estimation of the average contact pressure, $p_{\mathrm{cont,avg}}$. This was computed by temporally and spatially averaging the contact pressure at each of the four anterior-posterior locations according to

$$p_{\mathrm{cont,avg}_k} = \frac{1}{T_{\mathrm{close}_k}} \int_{t_{i_k}}^{t_{e_k}} \frac{1}{l_{\mathrm{cont,t}_k}(t)} \int_{x_{\mathrm{inf}_k}}^{x_{\mathrm{sup}_k}} p(x,t)\,\mathrm{d}x\,\mathrm{d}t, \tag{8}$$

where $p(x, t)$ indicates the intraglottal pressure at the inferior-superior location of x at time t, x_{sup} and x_{inf} are the inferior and superior margins of the contact region with a thickness equal to $l_{\mathrm{cont,t}}$, and the values t_i and t_e are the initial and ending time of the contact phase, respectively, with their difference equal to the duration of contact, T_{close}. The subscript k varies from 1 to 4 and denotes the location of the four anterior-posterior positions moving from the midline to the most anterior point, respectively.

The locations of the margins of contact were determined by identifying the spatial contact pressure distribution in the inferior-superior direction at each anterior location, as previously discussed. For example, the contact thickness is identified by the vertical dashed lines in Fig. 5 at time $t/T = 0.93$ along the glottal midline.

The time-varying contact thickness, $l_{\mathrm{cont,t}}$, is extracted from the experimental data and plotted in Fig. 6(a) as a function of normalized time at the four locations in the anterior-posterior direction. The temporal change in the contact area, A_{cont}, was calculated by integrating $l_{\mathrm{cont,t}}$ over the anterior-posterior length and is presented in Fig. 6(b) as a function of time. At each location, $l_{\mathrm{cont,t}}$ was shortest at the beginning of contact, and increased in time as the VF contacted the hemilarynx surface. The contact thickness remained largely constant during the remainder of contact, only decreasing slightly at the more central locations, prior to the end of contact. The average contact thickness as a function of anterior position is presented in Fig. 6(c), and is extrapolated to the anterior end point.

The tendency for the contact thickness not to decrease back to zero at the end of contact, as the VF begins to open, is likely a limitation of the method used for estimating the contact boundaries. That is, at the beginning and end of the contact phase, the pressure peaks observed in Fig. 3 are less pronounced, and it becomes difficult to discern the exact location of the inferior and superior edges of contact. More accurate measures to identify the contact margins could be

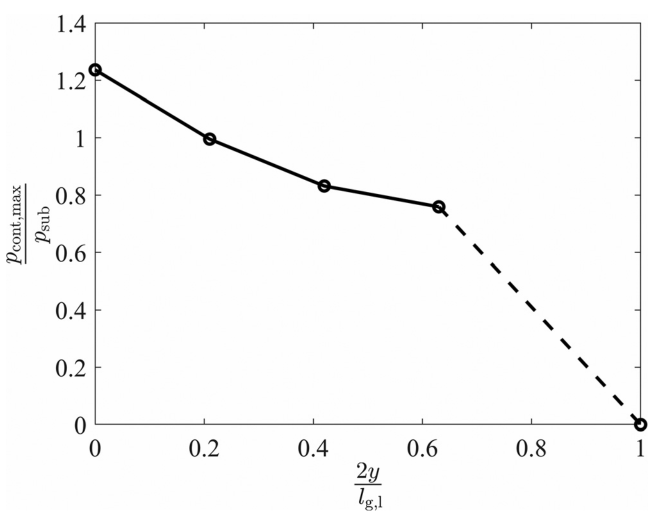

FIG. 4. The ratio of maximum contact pressure to subglottal pressure measured at various locations in the anterior-posterior direction.

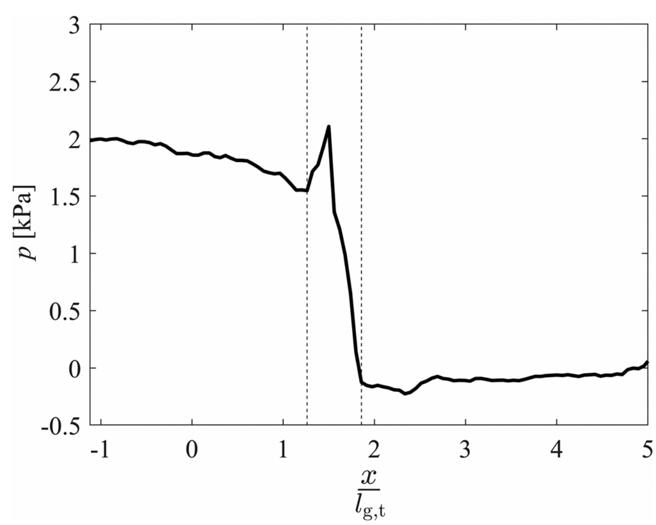

FIG. 5. Intraglottal pressure at the anterior-posterior midline of the VF at $t/T = 0.93$ with the inferior-superior contact region indicated by dashed lines.

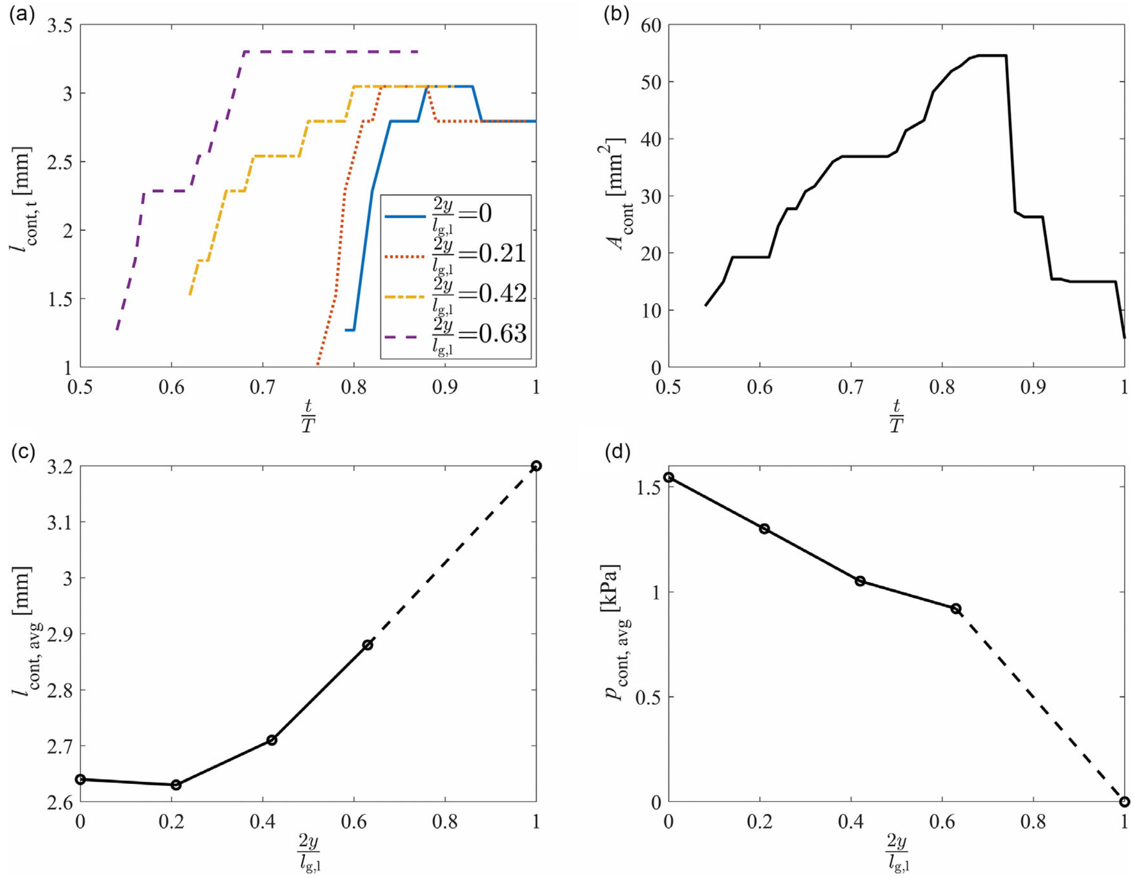

FIG. 6. (Color online) Temporal change in (a) contact thickness and (b) contact area. (c) Average contact thickness and (d) average contact pressure at each anterior-posterior location.

performed using previously employed approaches based on measuring changes to the electrical resistance of the VFs during contact.[16,46]

With the contact thickness, $l_{\text{cont,t}}$, estimated, the spatio-temporal mean of the contact pressure was computed from Eq. (8) at each anterior position and plotted in Fig. 6(d). The mean contact pressure was a maximum at the midline and decreased by approximately 35% at the most anterior location ($2y/l_{\text{g,l}} = 0.63$). This behavior is similar to the peak contact pressure (see Fig. 4). The ratio $p_{\text{cont,avg}_k}/p_{\text{cont,max}_k}$ is almost constant at about 0.57 across all of the anterior-posterior locations, denoting a linear relationship between peak and average contact pressure.

Finally, the average contact pressure over the entire contact area and period, $p_{\text{cont,avg}}$, was calculated by averaging the mean contact pressures over the anterior-posterior contact length. This was computed to be 0.87 kPa, yielding $p_{\text{cont,avg}}/p_{\text{cont,max}} = 0.32$ at the midline. Note, this value is 60% higher than the ratio of 0.20 that was proposed by Titze and Hunter[7] for estimating the average contact pressure from a known (i.e., measured) peak value. Calculating the standard deviation of the average contact pressure over the entire oscillation cycles is computationally cumbersome. Therefore, it can be reasonably approximated by considering the same ratio of standard deviation to average pressure found for $p_{\text{cont,max}}$. This gives a standard deviation of 0.02 kPa for $p_{\text{cont,avg}}$.

C. Dissipated-energy coefficient calculation

From the VF kinematics and the contact pressure data, the coefficient C can be computed from the values of $\dot{W}_{\text{k}}$, $\dot{W}_{\text{cont}}$, and $\dot{W}_{\text{d}}$, that were introduced in Sec. II.

1. Computing VF kinetic power

To calculate the VF kinetic power, $\dot{W}_{\text{k}}$, from Eq. (6), the VF geometry was approximated as a trapezoid with a medial thickness of $l_{\text{g,t}} = 4.26$ mm in the inferior-superior direction, lateral thickness of $l_{\text{la,t}} = 12.50$ mm in the inferior-superior direction, medial-lateral width of $l_{\text{VF,w}} = 7.50$ mm, and anterior-posterior length of $l_{\text{VF,l}} = 17.0$ mm. Therefore, the inferior-superior thickness of the trapezoid geometry can be expressed as $l_{\text{VF,t}}(z) = [(l_{\text{g,t}} - l_{\text{la,t}})/l_{\text{VF,w}}]z + l_{\text{la,t}}$ (note, the z coordinate is defined in Fig. 2). The VF has a coronal cross-sectional area of $A = 69.70$ mm^2. Based on these values, Eq. (6) can be evaluated, yielding $\dot{W}_{\text{k}} \approx (0.06/T)\rho V_{\text{cont}}^2$.

The VF medial surface velocity immediately preceding contact, V_{cont}, was estimated using the recorded HSV. The medial surface had a wave-like motion along the inferior-superior direction, such that the VF closure began at the inferior glottal edge and then progressed toward the superior edge. Therefore, the entire medial surface did not come into contact with the hemilaryngeal surface at once. The glottis had a divergent orientation during the closing phase, and the inferior edge of the VF was the visible VF boundary in the HSV. It was assumed that the medial surface velocity is constant along the inferior-superior direction and is equal to the velocity of the inferior edge. To find this velocity, kymograms were extracted at the four anterior-posterior locations at which the pressure data were acquired and a least-squares regression approach[47] was used to fit a sinusoidal function to the closing phase of each kymogram. The VF medial surface velocity at each location was computed from the derivative of this function over time, and the contact velocity was approximated as the VF surface velocity at the end of the closing phase (see Ref. 27 for more details). Averaging along the anterior-posterior direction, V_{cont} was calculated to be 0.58 m/s. The VF tissue density, ρ, was measured to be 1040 $\mathrm{kg/m^3}$. This resulted in $\dot{W}_{\mathrm{k}} \approx 3392.2\ \mathrm{W/m^3}$.

2. Computing contact power

Calculating the contact power, $\dot{W}_{\mathrm{cont}}$, from Eq. (7) requires calculation of $p_{\mathrm{cont,avg}}$, which was found in Sec. IV B 1, and estimation of the fictitious VF penetration distance, δ_{cont}. To estimate this latter value, a Hertzian contact model between two identical homogeneous elastic cylinders was employed[25] where the maximum contact pressure can be given by

$$\frac{p_{\max}}{E^*} = 4\frac{\delta_{\mathrm{cont}}}{l_{\mathrm{cont,t}}}, \tag{9}$$

where $p_{\max}$ is the maximum contact pressure, δ_{cont} is the penetration distance due to contact, $l_{\mathrm{cont,t}}$ is the contact thickness, and $E^* = E/2(1-\nu^2)$ is the effective Young's modulus defined where E is the equivalent Young's modulus of the layered VF structure, and ν is Poisson's ratio.

Because the silicone VF model consists of different layers of varying stiffness (see Fig. 2), the equivalent value of E is not known. Therefore, E^* was first computed using the known static prephonatory conditions of the VF. The VF had a medial-lateral width of $l_{\mathrm{VF,w}} = 7.50$ mm and an inferior-superior medial thickness of $l_{\mathrm{g,t}} = 4.26$ mm. In the compressed prephonatory orientation, the medial thickness in the inferior-superior direction, defined as $l_{\mathrm{pre,t}}$, was estimated by approximating the VF geometry as a deformed trapezoid that was compressed medially by 0.75 mm. This resulted in a value of $l_{\mathrm{pre,t}} = 6.12$ mm. The applied medial prephonatory pressure in this situation was 1.25 kPa. The VF contact behavior was modeled with a Hertzian contact model between two cylinders with the axial coordinate along the anterior-posterior direction. When at rest, the synthetic VF model had a flat medial surface, as opposed to the curved surface of a cylinder. To account for this discrete contact thickness at the onset of contact in the VF model, it was assumed that the cylinders were initially compressed in the medial direction such the resultant contact thickness was equal to the VF glottal thickness, $l_{\mathrm{g,t}}$, and then were further compressed by a pressure equal to the medial prephonatory pressure of the VF to create a contact thickness equal to the prephonatory medial thickness, $l_{\mathrm{pre,t}}$. Using these initial and prephonatory contact scenarios in Eq. (9) of the Hertzian contact model gives $E^* = 3.90$ kPa. This effective modulus falls within the span of the measured values of the elastic moduli measured for the different VF layers (see Table I).

With E^* estimated from the static measurements, the penetration depth during contact, δ_{cont}, was subsequently estimated using the same Hertzian model, except with the maximum contact pressure determined from the dynamic measurements. The mean values of the maximum contact pressure and contact thickness during the contact phase of the VF were calculated by averaging the magnitudes presented in Figs. 4 and 6(c) over the anterior-posterior contact length. They were found to be $p_{\mathrm{max,avg}} = 1.62$ kPa and $l_{\mathrm{cont,avg}} = 2.84$ mm, respectively. Using these quantities for $p_{\max}$ and $l_{\mathrm{cont,t}}$ in Eq. (9), and substituting the estimated value of $E^* = 3.90$ kPa, produced an estimate of the contact penetration depth of $\delta_{\mathrm{cont}} = 0.29$ mm.

Using the previously computed values for the average contact pressure, $p_{\mathrm{cont,avg}} = 0.87$ kPa, the fictitious penetration distance during contact, $\delta_{\mathrm{cont}} = 0.29$ mm, and the average contact area, $A_{\mathrm{cont,avg}} = l_{\mathrm{cont,avg}}\, l_{\mathrm{g,l}} = 48.28\ \mathrm{mm}^2$ and substituting them into Eq. (7), the contact power was found to be $\dot{W}_{\mathrm{cont}} = 1644.8\ \mathrm{W/m^3}$.

3. Computing dissipated power

The local dissipated power was computed based on the calculated values of $\dot{W}_{\mathrm{cont}}$ and $\dot{W}_{\mathrm{k}}$ according to $\dot{W}_{\mathrm{d}} = \dot{W}_{\mathrm{k}} - \dot{W}_{\mathrm{cont}}$, as previously introduced. The local dissipated power is plotted at each of the four anterior-posterior locations in Fig. 7. It can be seen that the dissipated power reaches the highest value along the VF midline and then decreases in the anterior direction. The dissipated power at $2y/l_{\mathrm{g,l}} = 0.63$ is 48% of the magnitude at the midline ($2y/l_{\mathrm{g,l}} = 0.0$). These findings help explain the prevalence of benign VF lesions forming along the midline of the glottis, as this is the region where the dissipated power is the highest.

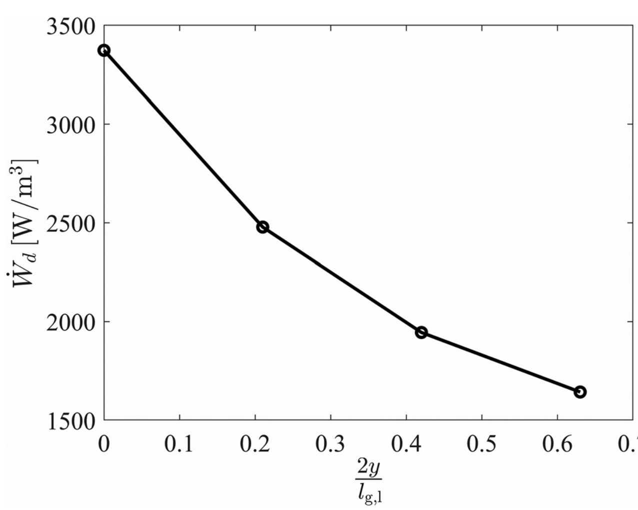

FIG. 7. Dissipated power per unit volume at various locations in the anterior-posterior direction.

Similarly, the average dissipated power across the entire VF surface during contact was computed and found to be $\dot{W}_{\mathrm{d}} = \dot{W}_{\mathrm{k}} - \dot{W}_{\mathrm{cont}} = 1747.4\ \mathrm{W/m^3}$.

With the average dissipated power known, the dissipation coefficient, C, was finally computed from Eq. (5) as $C = 0.52$. Note, this value is significantly higher than that estimated in the prior work of Titze and Hunter.[7] The implications are discussed next.

V. DISCUSSION

It has been proposed that the power dissipated within the VFs can lead to the formation of benign lesions.[5] Due to the difficulty in acquiring the contact pressure with the needed spatiotemporal resolution, correlations between the average and peak contact pressure have been estimated in prior studies, with the relationship that the average pressure is 20% of the peak pressure being previously suggested.[7] Quantitative measures of these values were performed in the current work, showing that the spatially and temporally-averaged contact pressure is 32% of the peak contact pressure, 60% higher than previously-reported approximations.[7] This difference is substantial, highlighting the importance of fully resolving the spatial and temporal variations in the contact pressure when computing the dissipated-energy/power dose. As the current work only investigated a single phonatory condition, it is expected that additional scenarios that depend on VF posturing (e.g., breathy versus pressed voice) as well as in the presence of benign lesions (e.g., nodules and polyps) will likely lead to different values. As such, care should be taken in estimating vocal dose measures based solely on peak contact pressure for a specific phonatory condition. It is interesting to note that the ratio of average pressure (in the inferior-superior direction) at a particular anterior-posterior location to the peak pressure at the same anterior-posterior location is largely constant across the VF length.

A coefficient that specifies the ratio of dissipated power to total power during VF collision, C, has been previously introduced as a parameter for estimating the VF energy-dissipation dose. The advantage in specifying the coefficient is that it allows estimation of VF dissipated power based solely on kinematic parameters of VF oscillation, which can be reliably estimated in the clinic. Unfortunately, prior work, suggesting a value of $C = 0.02$[7] was shown to be based upon a mathematical error and using an inaccurate assumption for computing the dissipated power. The current work corrected the mathematical error and revised the treatment to incorporate important physics that were neglected in the prior study. The value was estimated here to be $C = 0.52$, meaning that 52% of the total VF power prior to contact is dissipated during the collision phase, which is significantly larger than the previously proposed value, which indicated that VF collision was nearly a purely elastic phenomenon. The coefficient of restitution during VF collision can be approximated by taking the square root of the ratio of the kinetic power after contact to the kinetic power before contact. The dissipation coefficients of $C = 0.02$ obtained in the prior work[7] and $C = 0.52$ found in the current study, yield coefficients of restitution of $e \approx 0.99$ and $e \approx 0.69$, respectively. Studies of the coefficient of restitution in human tissue and cartilage have shown values to range between $e \approx 0.4$–0.76.[48,49] This indicates that the dissipation coefficient found using the updated model in this study is consistent with physiological values. It should be noted that the dissipation coefficient is likely to be influenced by the VF properties (i.e., geometry and material properties), and aerodynamics (i.e., subglottal pressure and flow rate). Therefore, the reported value for the dissipation coefficient should be interpreted within the constraints of the current work. The accuracy, and clinical relevance, of this work can be advanced in future studies by employing excised VFs to continue to explore these behaviors.

The updated dissipation coefficient also provides additional insights into vocal dose. The total dissipated power is the sum of power dissipated due to (1) internal friction during the non-contact phase of the VFs, and (2) the dissipated collision power, where only the second contribution has been considered in the current work. Prior work found the frictional dissipated power to be on the order of $100\ \mathrm{W/m^3}$ for females and $400\ \mathrm{W/m^3}$ for males.[7] These values were such that, using the previously proposed dissipation coefficient of $C = 0.02$ in Titze and Hunter,[7] the internal friction and dissipated collision power were of the same order of magnitude. However, with the updated value of $C = 0.52$ estimated herein, the dissipated collision power was found to be $\dot{W}_{\mathrm{d}} = 1747.4\,\mathrm{W/m^3}$, which is an order of magnitude greater than the estimated power dissipated due to friction. This suggests that collision is most likely the greatest contributor to VF damage during normal phonation, and that internal friction plays a secondary role. However, situations may arise (e.g., very high frequency during singing) where this relationship may change.

Using a Hertzian contact model to estimate the penetration distance of the VF assumes the VFs can be approximated as a cylinder.[25] Furthermore, the Hertzian contact model has been developed for static contact, does not include the effect of tissue inertia, and assumes that the material is purely elastic, whereas the VF tissue and the silicone rubber both have viscoelastic properties.[37,44] In spite of these limitations, it was found that the results obtained using this approach were reasonable. Nevertheless, implementing a viscoelastic model of contact to estimate the penetration depth during contact would provide a more accurate measure of the power dissipated during collision and is a focus of ongoing work. This advancement will also provide a more accurate prescription for modeling contact mechanics in numerical representations of VF collision.

Finally, the dissipation coefficient is also influenced by estimations of the VF kinetic power preceding contact. In the updated approach, a generalization of the medial surface velocity, and an estimation of how the VF velocity varies with medial-lateral depth, was utilized. More accurate estimates of the spatial variation of the VF velocity preceding contact are needed. The implementation of a finite element approach to estimate the total VF kinetic power could also yield useful advancements in the estimation of the dissipation coefficient.

VI. CONCLUSIONS

A synthetic self-oscillating VF model was implemented in a hemilaryngeal flow facility to measure the VF contact pressure and to estimate the contact dissipation dose with high temporal and spatial resolution. The oscillation kinematics of the VF model, such as frequency, open quotient, speed quotient, and glottal width, were found to be within the range of physiological values.

Analysis of the VF contact pressure showed that there is a spatial evolution of contact, occurring first at the anterior-posterior edges, and then progressing towards the midline. This behavior is indicative of the "zipper-like" closure that occurs *in vivo*. The contact area was found to have a crescent shape, closing at more inferior locations at the anterior/posterior edges and more superiorly at the midline. The peak contact pressure occurred along the mid anterior-posterior length of contact, with values that were representative of prior investigations. The peak contact pressure was 40% higher along the VF midline than at the most anterior position where the pressure was measured.

A previously proposed method for estimating contact dose was updated based on performing quantifiable measures of contact pressure and area. The average VF contact pressure was found to be 32% of the peak contact pressure, significantly higher than prior estimations. The percent of power dissipated due to VF collision was found to be 52% of the total VF power immediately preceding contact. These values provide useful information for clinical vocal dose investigations in which the measurement of average contact pressure is highly challenging. Nevertheless, additional phonatory conditions, including pathological ones, need to be investigated to explore these relationships over a broader range.

It was shown that for normal phonation, the collision dissipation dose is an order of magnitude higher than the shear dissipation dose that was reported in prior work.[7] This finding suggests that VF collision is the primary contributor to VF damage. In addition, the dissipated power was found to be highest along the midline of the VF, consistent with clinical observations that this is the location where benign VF lesions are most likely to occur.

ACKNOWLEDGMENTS

This research was supported by the National Institutes of Health (NIH) National Institute on Deafness and other Communication Disorders Grant Nos. P50 DC015446 and ANID BASAL FB0008. The content is solely the responsibility of the authors and does not necessarily represent the official views of the National Institutes of Health.

[1]I. R. Titze, "Mechanical stress in phonation," J. Voice **8**(2), 99–105 (1994).
[2]T. Kojima, M. Van Deusen, W. G. Jerome, C. G. Garrett, M. P. Sivasankar, C. K. Novaleski, and B. Rousseau, "Quantification of acute vocal fold epithelial surface damage with increasing time and magnitude doses of vibration exposure," PLoS One **9**(3), e91615 (2014).
[3]R. E. Hillman, C. E. Stepp, J. H. Van Stan, M. Zañartu, and D. D. Mehta, "An updated theoretical framework for vocal hyperfunction," Am. J. Speech Lang. Pathol. **29**(4), 2254–2260 (2020).
[4]J. J. Jiang and I. R. Titze, "Measurement of vocal fold intraglottal pressure and impact stress," J. Voice **8**, 132–144 (1994).
[5]I. R. Titze, J. G. Svec, and P. S. Popolo, "Vocal dose measures," J. Speech Lang. Hear. Res. **46**, 919–932 (2003).
[6]J. H. Van Stan, D. D. Mehta, A. J. Ortiz, J. A. Burns, K. L. Marks, L. E. Toles, T. Stadelman-Cohen, C. Krusemark, J. Muise, T. Hron, S. Zeitels, A. B. Fox, and R. E. Hillman, "Changes in a daily phonotrauma index (DPI) after laryngeal surgery and voice therapy: Implications for the role of daily voice use in the etiology and pathophysiology of phonotraumatic vocal hyperfunction," J. Speech Lang. Hear. Res. **63**(12), 3934–3944 (2020).
[7]I. R. Titze and E. J. Hunter, "Comparison of vocal vibration-dose measures for potential-damage risk criteria," J. Speech Lang. Hear. Res. **58**(5), 1425–1439 (2015).
[8]K. Verdolini and L. O. Ramig, "Occupational risks for voice problems," Logoped. Phoniatr. Vocol. **26**(1), 37–46 (2001).
[9]L. Rantala and E. Vilkman, "Relationship between subjective voice complaints and acoustic parameters in female teachers' voices," J. Voice **13**(4), 484–495 (1999).
[10]F. Alipour and R. C. Scherer, "Dynamic glottal pressures in an excised hemilarynx model," J. Voice **14**(4), 443–454 (2000).
[11]L. Chen and L. Mongeau, "Verification of two minimally invasive methods for the estimation of the contact pressure in human vocal folds during phonation," J. Acoust. Soc. Am. **130**(3), 1618–1627 (2011).
[12]M. M. Hess, K. Verdolini, W. Bierhals, U. Mansmann, and M. Gross, "Endolaryngeal contact pressures," J. Voice **12**, 50–67 (1998).
[13]K. Verdolini, R. Chan, I. R. Titze, M. Hess, and W. Bierhals, "Correspondence of electroglottographic closed quotient to vocal fold impact stress in excised canine larynges," J. Voice **12**(4), 415–423 (1998).
[14]K. Verdolini, M. M. Hess, I. R. Titze, W. Bierhals, and M. Gross, "Investigation of vocal fold impact stress in human subjects," J. Voice **13**(2), 184–202 (1999).
[15]H. E. Gunter, R. D. Howe, S. M. Zeitels, J. B. Kobler, and R. E. Hillman, "Measurement of vocal fold collision forces during phonation," J. Speech Lang. Hear. Res. **48**(3), 576 (2005).
[16]M. Motie-Shirazi, M. Zañartu, S. D. Peterson, D. D. Mehta, J. B. Kobler, R. E. Hillman, and B. D. Erath, "Toward development of a vocal fold contact pressure probe: Sensor characterization and validation using synthetic vocal fold models," Appl. Sci. **9**(15), 3002 (2019).
[17]D. D. Mehta, J. B. Kobler, S. M. Zeitels, M. Zañartu, B. D. Erath, M. Motie-Shirazi, S. D. Peterson, R. H. Petrillo, and R. E. Hillman, "Toward development of a vocal fold contact pressure probe: Bench-top validation of a dual-sensor probe using excised human larynx models," Appl. Sci. **9**(20), 4360 (2019).
[18]H. Bakhshaee, J. Young, J. C. Yang, L. Mongeau, and A. K. Miri, "Determination of strain field on the superior surface of excised larynx vocal folds using dic," J. Voice **27**(6), 659–667 (2013).
[19]S. Weiss, A. Sutor, S. J. Rupitsch, S. Kniesburges, M. Döllinger, and R. Lerch, "Development of a small film sensor for the estimation of the contact pressure of artificial vocal folds," in *Proceedings of Meetings on Acoustics ICA2013*, Montreal, Canada (June 2–7, 2013), p. 060307.
[20]M. Spencer, T. Siegmund, and L. Mongeau, "Determination of superior surface strains and stresses, and vocal fold contact pressure in a synthetic larynx model using digital image correlation," J. Acoust. Soc. Am. **123**(2), 1089–1103 (2008).
[21]C. Tao and J. J. Jiang, "Mechanical stress during phonation in a self-oscillating finite-element vocal fold model," J. Biomech. **40**, 2191–2198 (2007).
[22]P. Bhattacharya and T. Siegmund, "A computational study of systemic hydration in vocal fold collision," Comput. Methods Biomech. Biomed. Eng. **17**(16), 1835–1852 (2014).

[23]Z. Zhang, "Vocal fold contact pressure in a three-dimensional body-cover phonation model," J. Acoust. Soc. Am. **146**(1), 256–265 (2019).
[24]P. J. Hadwin, M. Motie-Shirazi, B. D. Erath, and S. D. Peterson, "Bayesian inference of vocal fold material properties from glottal area waveforms using a 2D finite element model," Appl. Sci. **9**(13), 2735 (2019).
[25]M. E. Díaz-Cádiz, S. D. Peterson, G. E. Galindo, V. M. Espinoza, M. Motie-Shirazi, B. D. Erath, and M. Zañartu, "Estimating vocal fold contact pressure from raw laryngeal high-speed videoendoscopy using a Hertz contact model," Appl. Sci. **9**(11), 2384 (2019).
[26]A. H. Mendelsohn and Z. Zhang, "Phonation threshold pressure and onset frequency in a two-layer physical model of the vocal folds," J. Acoust. Soc. Am. **130**(5), 2961–2968 (2011).
[27]M. Motieshirazi, M. Zañartu, S. D. Peterson, and B. D. Erath, "Intraglottal aerodynamic pressure and energy transfer in a self-oscillating synthetic model of the vocal folds," medRxiv (2020).
[28]B. H. Story, "Comparison of magnetic resonance imaging-based vocal tract area functions obtained from the same speaker in 1994 and 2002," J. Acoust. Soc. Am. **123**(1), 327–335 (2008).
[29]M. Döllinger, D. A. Berry, and D. W. Montequin, "The influence of epilarynx area on vocal fold dynamics," Otolaryngol. Head Neck Surg. **135**(5), 724–729 (2006).
[30]K. Comley and N. Fleck, "The compressive response of porcine adipose tissue from low to high strain rate," Int. J. Impact Eng. **46**, 1–10 (2012).
[31]Y. B. Min, I. R. Titze, and F. Alipour-Haghighi, "Stress-strain response of the human vocal ligament," Ann. Otol. Rhinol. Laryngol. **104**(7), 563–569 (1995).
[32]D. K. Chhetri, Z. Zhang, and J. Neubauer, "Measurement of Young's modulus of vocal folds by indentation," J. Voice **25**, 1–7 (2011).
[33]G. R. Dion, P. G. Coelho, S. Teng, M. N. Janal, M. R. Amin, and R. C. Branski, "Dynamic nanomechanical analysis of the vocal fold structure in excised larynges," Laryngoscope **127**(7), E225–E230 (2017).
[34]F. Alipour and S. Vigmostad, "Measurement of vocal folds elastic properties for continuum modeling," J. Voice **26**(6), 816–821 (2012).
[35]R. W. Chan and I. R. Titze, "Viscoelastic shear properties of human vocal fold mucosa: Measurement methodology and empirical results," J. Acoust. Soc. Am. **106**, 2008–2021 (1999).
[36]R. W. Chan, M. Fu, L. Young, and N. Tirunagari, "Relative contributions of collagen and elastin to elasticity of the vocal fold under tension," Ann. Biomed. Eng. **35**(8), 1471–1483 (2007).
[37]R. W. Chan and M. L. Rodriguez, "A simple-shear rheometer for linear viscoelastic characterization of vocal fold tissues at phonatory frequencies," J. Acoust. Soc. Am. **124**(2), 1207–1219 (2008).
[38]L. Oren, D. Dembinski, E. Gutmark, and S. Khosla, "Characterization of the vocal fold vertical stiffness in a canine model," J. Voice **28**(3), 297–304 (2014).
[39]R. E. Kania, S. Hans, D. M. Hartl, P. Clement, L. Crevier-Buchman, and D. F. Brasnu, "Variability of electroglottographic glottal closed quotients: Necessity of standardization to obtain normative values," Arch. Otolaryngol. Head Neck Surg. **130**(3), 349–352 (2004).
[40]J. Lohscheller, J. G. Švec, and M. Döllinger, "Vocal fold vibration amplitude, open quotient, speed quotient and their variability along glottal length: Kymographic data from normal subjects," Logoped. Phoniatr. Vocol. **38**(4), 182–192 (2013).
[41]M. Döllinger and D. A. Berry, "Visualization and quantification of the medial surface dynamics of an excised human vocal fold during phonation," J. Voice **20**(3), 401–413 (2006).
[42]I. R. Titze and F. Alipour, *The Myoelastic Aerodynamic Theory of Phonation* (National Center for Voice and Speech, Salt Lake City, UT, 2006).
[43]R. J. Baken and R. F. Orlikoff, *Clinical Measurement of Speech and Voice* (Cengage Learning, Boston, MA, 2000).
[44]P. R. Murray and S. L. Thomson, "Vibratory responses of synthetic, self-oscillating vocal fold models," J. Acoust. Soc. Am. **132**(5), 3428–3438 (2012).
[45]See Supplementary materials at https://doi.org/10.1121/10.0005596 for a video showing the progression of the intraglottal pressure distribution.
[46]K. L. Syndergaard, S. Dushku, and S. L. Thomson, "Electrically conductive synthetic vocal fold replicas for voice production research," J. Acoust. Soc. Am. **142**(1), EL63–EL68 (2017).
[47]J. J. Jiang, Y. Zhang, M. P. Kelly, E. T. Bieging, and M. R. Hoffman, "An automatic method to quantify mucosal waves via videokymography," Laryngoscope **118**(8), 1504–1510 (2008).
[48]L. Edelsten, J. E. Jeffrey, L. V. Burgin, and R. M. Aspden, "Viscoelastic deformation of articular cartilage during impact loading," Soft Mater. **6**(20), 5206–5212 (2010).
[49]K. Anderson, J. Oleson, and T. Anthony, "Variability in coefficient of restitution in human facial skin," Skin. Res. Technol. **20**(3), 355–362 (2014).